



Article

# State-of-Charge Estimation of Lithium-Ion Battery Based on Convolutional Neural Network Combined with Unscented Kalman Filter

Hongli Ma <sup>1</sup>, Xinyuan Bao <sup>1,\*</sup> ID, António Lopes <sup>2,\*</sup> ID, Liping Chen <sup>1</sup> ID, Guoquan Liu <sup>3</sup> and Min Zhu <sup>1</sup>

<sup>1</sup> School of Electrical Engineering and Automation, Hefei University of Technology, Hefei 230009, China; 2023010050@mail.hfut.edu.cn (H.M.); lip\_chen@hfut.edu.cn (L.C.); zhumin71@126.com (M.Z.)

<sup>2</sup> LAETA/INEGI, Faculty of Engineering, University of Porto, Rua Dr. Roberto Frias, 4200-465 Porto, Portugal

<sup>3</sup> School of Mechanical and Electronic Engineering, East China University of Technology, Nanchang 330013, China; gqlecit@hotmail.com

\* Correspondence: 2020010034@mail.hfut.edu.cn (X.B.); aml@fe.up.pt (A.L.)

**Abstract:** Estimation of the state-of-charge (SOC) of lithium-ion batteries (LIBs) is fundamental to assure the normal operation of both the battery and battery-powered equipment. This paper derives a new SOC estimation method (CNN-UKF) that combines a convolutional neural network (CNN) and an unscented Kalman filter (UKF). The measured voltage, current and temperature of the LIB are the input of the CNN. The output of the hidden layer feeds the linear layer, whose output corresponds to an initial network-based SOC estimation. The output of the CNN is then used as the input of a UKF, which, using self-correction, yields high-precision SOC estimation results. This method does not require tuning of network hyperparameters, reducing the dependence of the network on hyperparameter adjustment and improving the efficiency of the network. The experimental results show that this method has higher accuracy and robustness compared to SOC estimation methods based on CNN and other advanced methods found in the literature.



**Citation:** Ma, H.; Bao, X.; Lopes, A.; Chen, L.; Liu, G.; Zhu, M.

State-of-Charge Estimation of Lithium-Ion Battery Based on Convolutional Neural Network Combined with Unscented Kalman Filter. *Batteries* **2024**, *10*, 198. <https://doi.org/10.3390/batteries10060198>

Academic Editor: Pascal Venet

Received: 29 April 2024

Revised: 29 May 2024

Accepted: 31 May 2024

Published: 4 June 2024



**Copyright:** © 2024 by the authors. Licensee MDPI, Basel, Switzerland. This article is an open access article distributed under the terms and conditions of the Creative Commons Attribution (CC BY) license (<https://creativecommons.org/licenses/by/4.0/>).

## 1. Introduction

To improve energy efficiency and limit greenhouse emissions, the international community has been committed to deploying electric vehicles (EVs) [1]. Energy storage equipment is crucial in EVs, with lithium-ion batteries (LIBs) being the most used, thanks to their long life cycle and high energy density [2–5]. The state-of-charge (SOC) of a battery, specified as the ratio of its remaining capacity to its fully charged state capacity, is a fundamental index to assess the condition of the battery. Therefore, the SOC varies between 0 and 1, the lower and higher limits corresponding to fully discharged and fully charged states [6]. Accurate estimation of the SOC is crucial for EVs, being used by the battery management system (BMS) to prevent over-discharging and over-charging and, ultimately, to guarantee the reliability and safe operation of EVs [7–9]. However, the SOC is not directly measurable, being indirectly determined through acquired sensory data, namely battery voltage, current and temperature, and some suitable data processing method [10]. Currently, commonly used methods for determining the SOC include open circuit voltage (OCV), current integration, model-based and data-driven ones. The OCV technique is simple, but leads to large errors [11]. The current integration method may yield high accuracy, but it is affected by cumulative errors, and the SOC initial value cannot be determined [12]. The model-based approaches often rely on complex equivalent circuit models (ECMs) and Kalman filters (KFs) to estimate SOC online [4,13]. Common variants adopt the unscented KF (UKF) [14] or the extended KF (EKF) [15]. However, as the chemical processes internal to the battery are complex, it is difficult to establish ECMs that completely describe its internal behavior,

which limits the accuracy of SOC determination. The data-driven methods only need external measurable data of the battery, which are then used by machine learning procedures that automatically learn the relationship among the input data and the SOC value, without knowing information concerning internal battery reactions [16,17]. Neural networks have been commonly adopted as data-driven methods for estimating the SOC of LIBs, including gated recurrent units (GRUs), long short-term memory (LSTM) and convolutional neural networks (CNNs), among others. For example, references [18,19] adopted a GRU for SOC estimation, Ref. [20] used an LSTM network and [21,22] derived a method based on CNNs. In addition to using single neural networks for SOC estimation, some studies have proposed combining different neural network models. For example, Refs. [23,24] used a combination of CNNs and LSTM, and Ref. [25] proposed a CNN-GRU-LSTM joint method. Even though some existing methods can achieve good SOC estimation results, most single neural network-based ones reveal certain limitations. Indeed, the hyperparameters of neural networks are complex and their adjustment requires considerable time. Additionally, when the hyperparameters are not properly selected, the generalization performance of the model is compromised, resulting in poor estimation results. Methods that combine different neural networks can obtain better SOC estimation, but increasing the depth of the model will increase complexity and the number of hyperparameters, making it more difficult to adjust and taking longer to make predictions.

This paper gives a contribution to mitigate the above issues, by proposing an SOC estimation method of LIBs that combines a CNN and a UKF. The new CNN-UKF method uses measurable features of the LIB, namely voltage, current and temperature, as the input of a CNN. The data are processed through the hidden and linear layers to output SOC estimation results. Then, this output is used as the input of a UKF, which uses self-correction to obtain the final SOC values. Experiments are provided to show that the new CNN-UKF method is robust to model hyperparameters, and yields good results in multiple sets of experiments without changing the hyperparameters of the neural network. The adoption of a UKF significantly improves the estimation accuracy. The CNN-UKF approach does not require detailed knowledge on the neural network model, and possesses strong prediction stability and generalization capabilities. Compared with other data-driven methods, the CNN-UKF yields superior performance.

The rest of this paper includes Section 2, which introduces the CNN-UKF methodology, Section 3 devoted to the experimental results and, finally, Section 4, which gives a summary of the main findings.

## 2. Methodology

Figure 1 illustrates the overall flowchart of the proposed CNN-UKF. The measured voltage, current and temperature,  $V$ ,  $I$  and  $T$ , respectively, of the battery are input into the CNN layer and the pooling layer to obtain the hidden features. Their output is then used to feed the fully connected layer to further extract features and obtain an estimation of the SOC. This SOC predicted value is filtered using a UKF, and the final SOC estimation result is obtained.

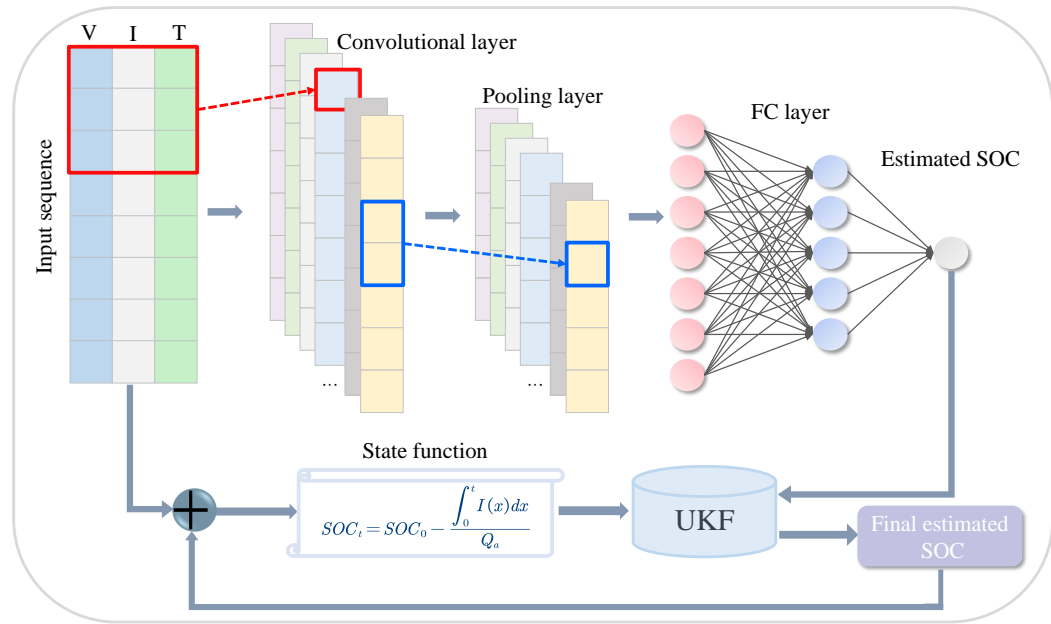


**Figure 1.** Overall flowchart of CNN-UKF.

### 2.1. The 1D CNN

Data concerning the SOC of LIBs is sequential and highly correlated with time. A 1-dimensional (1D) CNN can be used to effectively extract features of time-series and, therefore, is adopted herein. The layout of the 1D CNN is illustrated in Figure 1. Within the convolutional layer, the convolution operation can be described by:

$$c_t = f_{cnn}(W_{cnn} * \omega_t + b_{cnn}), \quad (1)$$

where  $f_{cnn}(\cdot)$  represents the activation function,  $W_{cnn}$  and  $b_{cnn}$  correspond to the weight coefficient and bias parameter, respectively,  $\omega_t$  is the  $t$ -th sample input information,  $*$  stands for the convolution operation and  $c_t$  represents the output after convolution. The pooling layer performs feature selection on the output of the convolutional layer. The selected features enter the fully connected layer, which outputs a predicted SOC value. As this initially estimated SOC is largely affected by noise, a UKF is adopted to enhance the accuracy of the SOC estimation.

### 2.2. The UKF

The process of using a UKF to filter data and estimate SOC is as follows [13]:

- (1) Let us consider that the mean value of the state variable is  $\bar{x}$ , the variance is  $P$ , and the expected value is  $E$ . Initialize the mean and variance:

$$\hat{x}_0 = E[x_0], \quad (2)$$

$$P_0 = E[(x_0 - \hat{x}_0)(x_0 - \hat{x}_0)^T]. \quad (3)$$

(2) Obtain the sigma point set and weight value:

$$\begin{cases} \mathcal{Y}_{i,t-1} = \hat{x}_{t-1}, j = 0, \\ \mathcal{Y}_{i,t-1} = \hat{x}_{t-1} + \left( \sqrt{(n + \kappa) P_{\mathcal{Y},t-1}} \right)_i, \\ \quad j = 1, 2, \dots, n, \\ \mathcal{Y}_{i,t-1} = \hat{x}_{t-1} - \left( \sqrt{(n + \kappa) P_{\mathcal{Y},t-1}} \right)_i, \\ \quad j = n + 1, n + 2, \dots, 2n, \end{cases} \quad (4)$$

where  $\kappa$  represents the proportion modification parameter. The mean weight and covariance weight,  $\theta_m$  and  $\theta_c$ , respectively, can be calculated by:

$$\begin{cases} \theta_m^{(0)} = \frac{\kappa}{n + \kappa}, \\ \theta_c^{(0)} = \frac{\kappa}{n + \kappa} + 1 - \lambda^2 + \beta, \\ \theta_m^{(j)} = \theta_c^{(j)} = \frac{\kappa}{2(n + \kappa)}, j = 1, \dots, 2n. \end{cases} \quad (5)$$

(3) Calculate the one-step prediction of  $\mathcal{Y}$ , and update the prediction value and the covariance matrix,  $\hat{\mathcal{Y}}_{t|t-1}^{(j)}$  and  $P_{t|t-1}$ , respectively:

$$\begin{cases} \mathcal{Y}_{t|t-1}^{(i)} = h(\mathcal{Y}_{t-1}^{(j)}), \\ \hat{\mathcal{Y}}_{t|t-1} = \sum_{j=0}^{2n} \theta_m^{(j)} \mathcal{Y}_{t|t-1}^{(j)}, \\ P_{t|t-1} = \sum_{j=0}^{2n} \theta_c^{(j)} (\mathcal{X}_{t|t-1}^{(j)} - \hat{\mathcal{Y}}_{t|t-1}) \cdot \\ \quad (\mathcal{Y}_{t|t-1}^{(j)} - \hat{\mathcal{Y}}_{t|t-1})^T + Q_t, \end{cases} \quad (6)$$

where  $h(\cdot)$  represents the state equation, and  $Q_t$  represents the process noise covariance.

(4) Find the predicted value  $X_t$  and the predicted mean  $\hat{X}_t$ :

$$\begin{cases} X_t^{(j)} = f(\mathcal{Y}_{t-1}^{(j)}), \\ \hat{X}_t = \sum_{j=0}^{2n} \theta_m^{(j)} X_t^{(j)}, \end{cases} \quad (7)$$

where  $f(\cdot)$  represents the measurement equation.

(5) Find the predicted covariance:

$$\begin{cases} P_{yy} = \sum_{j=0}^{2n} \theta_c^{(j)} (X_t^{(j)} - \hat{X}_t) \cdot \\ \quad (X_t^{(j)} - \hat{X}_t)^T + N_t, \\ P_{xy} = \sum_{i=0}^{2n} \theta_c^{(j)} (\mathcal{Y}_{t|t-1}^{(j)} - \hat{\mathcal{Y}}_{t|t-1}) \cdot \\ \quad (\mathcal{Y}_{t|t-1}^{(j)} - \hat{\mathcal{Y}}_{t|t-1})^T, \end{cases} \quad (8)$$

where  $N_t$  represents the measurement noise covariance.

(6) Find the Kalman gain:

$$\Gamma(t+1) = P_{xy}P_{yy}^{-1}. \quad (9)$$

(7) Finally, update the state and covariance matrices:

$$\begin{cases} \hat{Y}_{t|t} = \hat{Y}_{t|t-1} + \Gamma(t)(X_t - \hat{X}_{t|t-1}), \\ P_{t|t} = P_{t|t-1} - \Gamma(t)P_{yy}\Gamma(t)^T. \end{cases} \quad (10)$$

In this study, we consider the UKF state equation as:

$$SOC_t = SOC_{t-1} - \frac{I_{t-1}\Delta t}{Q_a} + Q_t, \quad (11)$$

where  $\Delta t$  represents the time interval, and  $Q_a$  and  $Q_t$  represent the maximum capacity of the LIB and the process noise covariance of the SOC at the time instant  $t$ , respectively.

The measurement equation of the UKF is given by:

$$Y_t = \widehat{SOC}_t + R_t, \quad (12)$$

where  $\widehat{SOC}_t$  stands for the value determined by the CNN model, and  $R_t$  represents the measurement noise covariance of the SOC at time  $t$ . The UKF has a self-correction capability, which confers higher accuracy and robustness to the CNN-UKF scheme.

### 3. Experiments

#### 3.1. Datasets and Experimental Evaluation Criteria

For the experiments we adopt the Panasonic LIBs dataset [26], which is commonly used to evaluate SOC estimation methods. This dataset includes batteries' information collected at five values of temperature ( $-20^{\circ}\text{C}$ ,  $-10^{\circ}\text{C}$ ,  $0^{\circ}\text{C}$ ,  $10^{\circ}\text{C}$  and  $25^{\circ}\text{C}$ ) and nine vehicle driving conditions (Cycle\_1, Cycle\_2, Cycle\_3, Cycle\_4, NN, HWFET, LA92, UDDS and US06) for each temperature. Among these driving cycles, HWFET simulates highway driving conditions, UDDS is an urban driving schedule test and LA92 includes more complex speed and acceleration variations, simulating the actual urban driving conditions in the Los Angeles area. US06 is a supplemental test cycle used to evaluate the fuel economy and emissions of vehicles under high acceleration, high-speed driving and rapid speed changes. NN consists of US06 and LA92, while Cycle1-Cycle4 are random combinations of HWFET, US06, UDDS, NN and LA92. Batteries' data are available at a sampling interval of 0.1 s.

Figure 2 shows the variation in  $V$ ,  $I$  and  $T$  for the NN and the LA92 operating conditions, under the temperatures  $25^{\circ}\text{C}$ ,  $10^{\circ}\text{C}$  and  $0^{\circ}\text{C}$ . We can see that, for distinct driving cycles,  $V$ ,  $I$  and  $T$  exhibit large differences. Moreover, for the same driving cycle, the values of the features also show substantial discrepancies. To mitigate the influence of the measurement units and magnitude of the features, we normalize the data, using:

$$D_{norm} = \frac{D - D_{\min}}{D_{\max} - D_{\min}}, \quad (13)$$

where  $D$  represents original data, with minimum and maximum values  $D_{\min}$  and  $D_{\max}$ , respectively, and  $D_{norm}$  represents the normalized values. Through normalization, the differences between data can be reduced, helping the network model during the learning process.

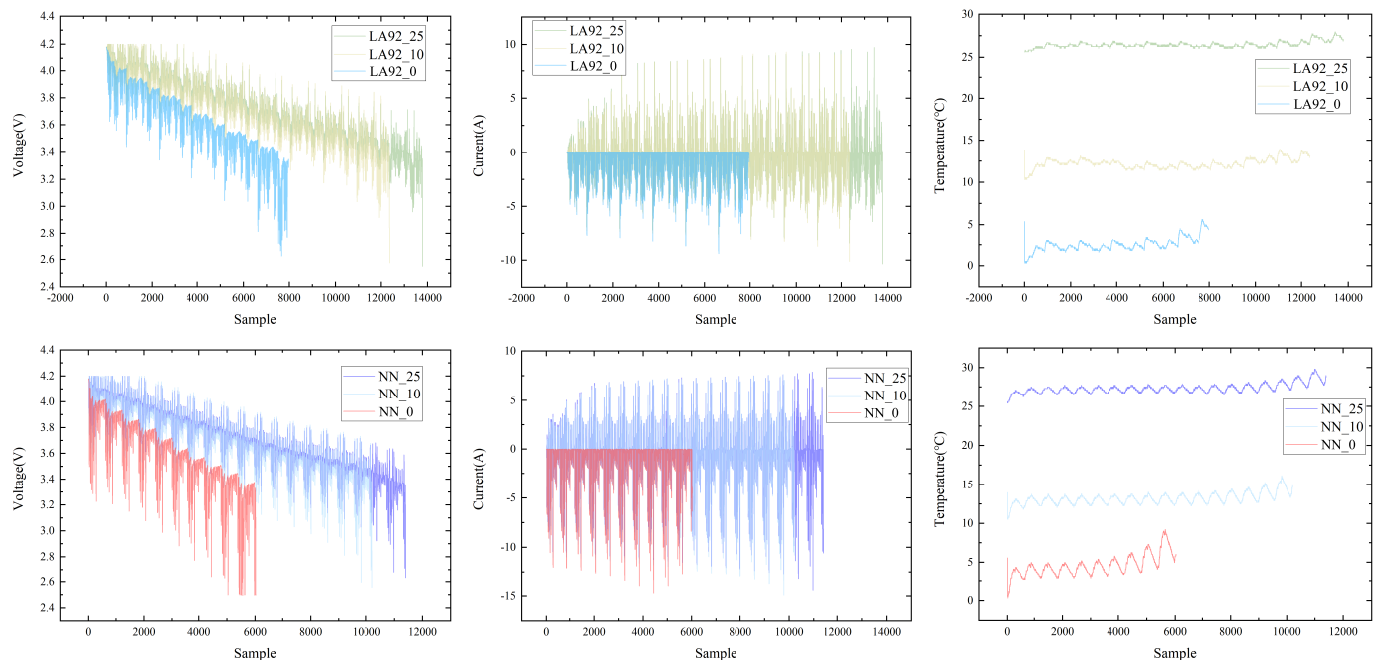


**Figure 2.** Trends in various characteristics at different temperatures under NN and LA92 operating conditions.

To assess the accuracy of the SOC estimation methods, we adopt the root mean square error (RMSE) and the mean absolute error (MAE) indices, which are given by:

$$RMSE = \sqrt{\frac{1}{L} \sum_{n=1}^L (y_n - \hat{y}_n)^2}, \quad (14)$$

$$MAE = \frac{1}{L} \sum_{n=1}^L |y_n - \hat{y}_n|, \quad (15)$$

where  $L$  corresponds to the number of points of the sequence, and  $y_n$  and  $\hat{y}_n$  represent the real and estimated SOC values, respectively. In this paper, the real value is obtained through the ampere-hour integration method.

### 3.2. Comparison and Analysis of Different Methods

To verify the effectiveness of the CNN-UKF method, we test different driving conditions at different temperatures. The input of the CNN-UKF model consists of the batteries' data  $V$ ,  $I$  and  $T$ , while the output is the SOC. For every experiment, one of the driving cycles' datasets is selected as the test set, and the remaining driving cycles' datasets serve as the training set. We do not change the hyperparameters' settings of the CNN model, which saves much time during the hyperparameters' tuning. In the comparison experiment in this section, the initial value of the measurement noise covariance matrix ( $R$ ) of UKF is set to  $1 \times 10^0$  (1e0). Figures 3–6 compare the results of the CNN and CNN-UKF methods under UDDS, US06, NN and LA92 driving conditions. We verify that the estimation error of the CNN model fluctuates up and down. The SOC, being highly correlated with time, shows uneven characteristics. Conversely, the CNN-UKF results are significantly smoother and maintained at a lower error level, thanks to the filtering action of the output of the CNN.

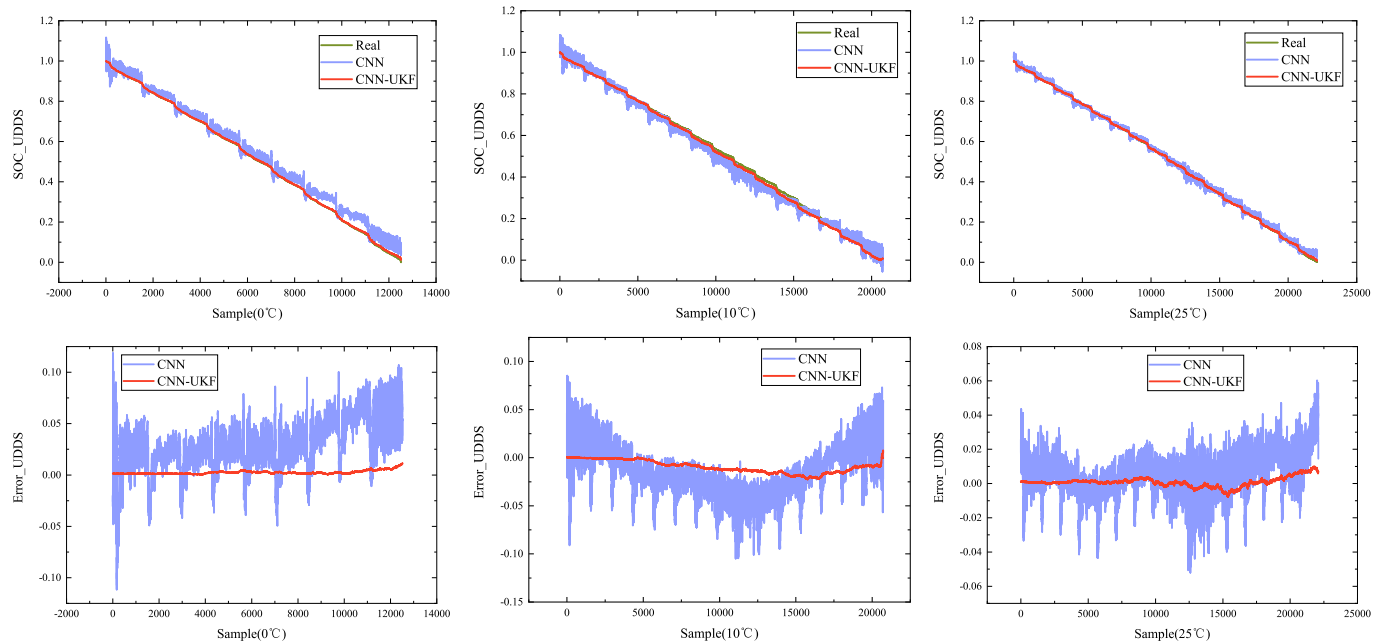


**Figure 3.** Experimental results of the CNN and CNN-UKF, under distinct temperatures and the UDDS driving cycle.

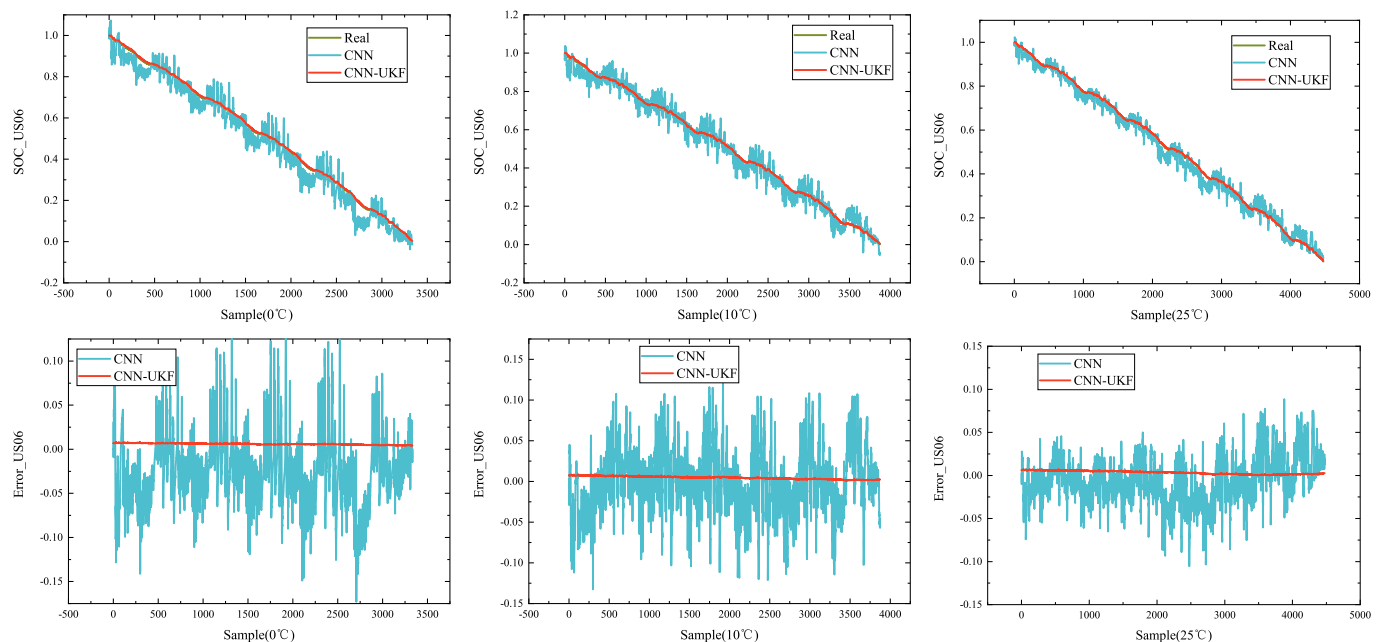


**Figure 4.** Experimental results of the CNN and CNN-UKF, under distinct temperatures and the US06 driving cycle.

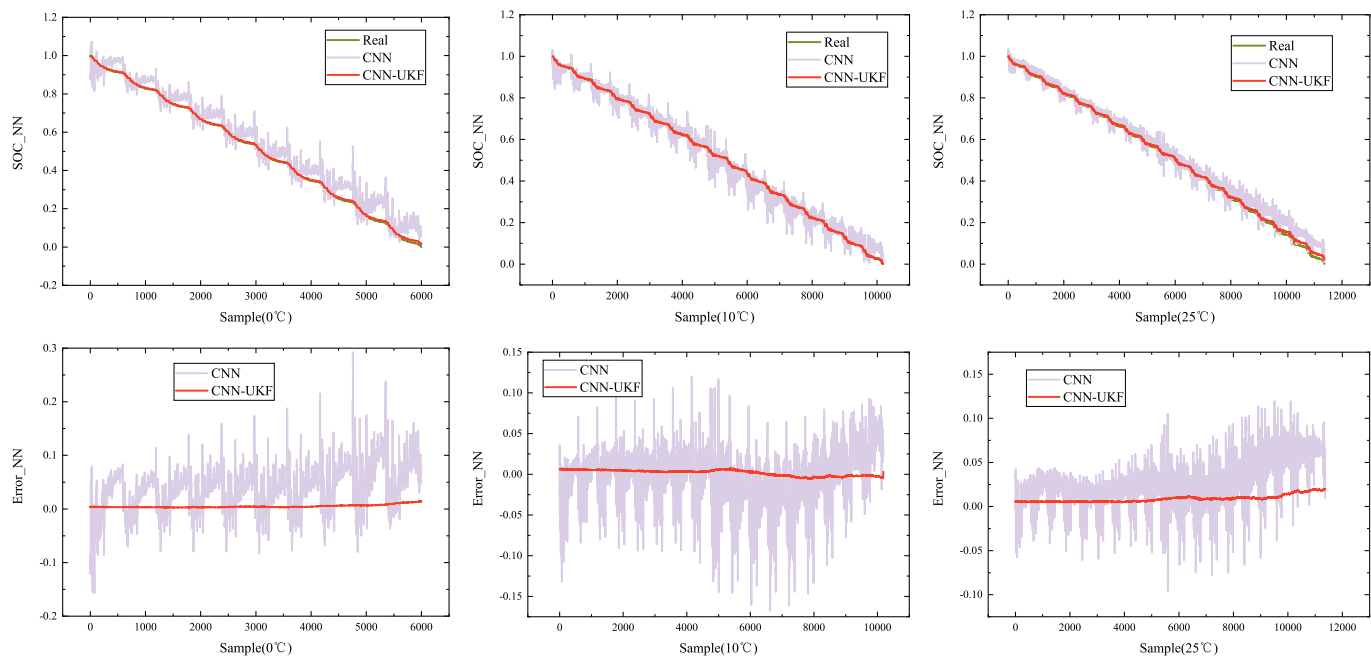


**Figure 5.** Experimental results of the CNN and CNN-UKF, under distinct temperatures and the NN driving cycle.

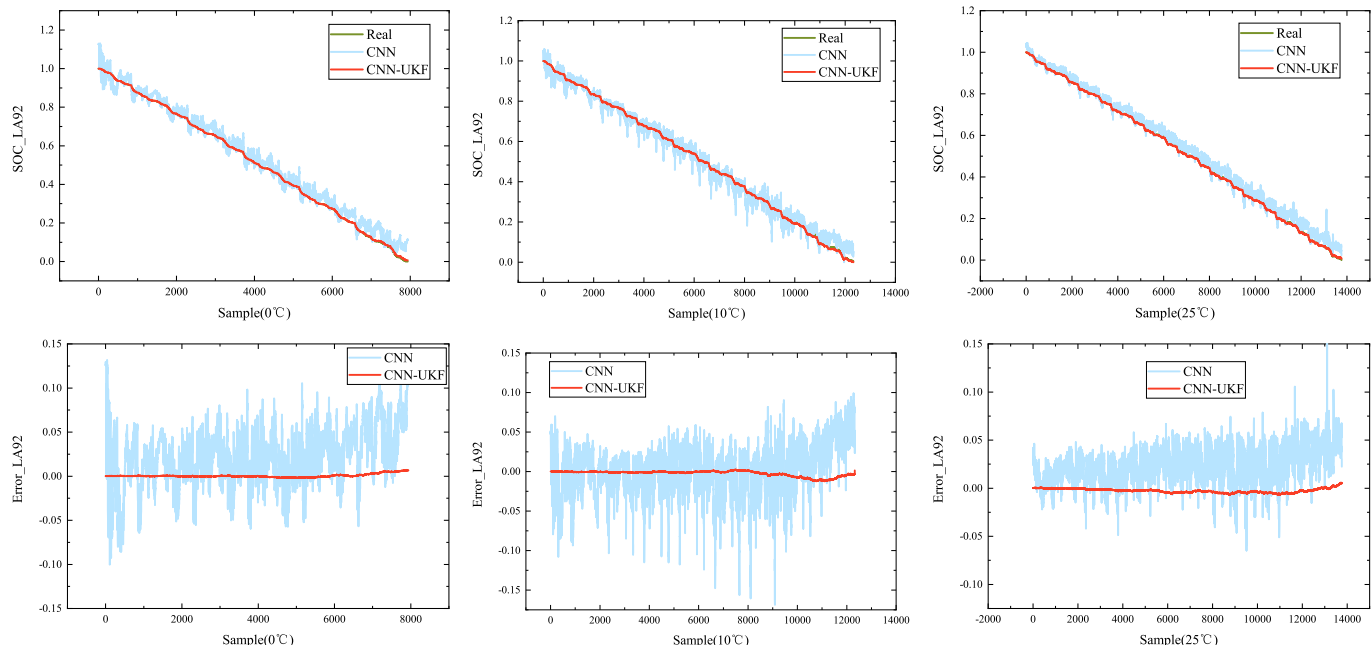


**Figure 6.** Experimental results of the CNN and CNN-UKF, under distinct temperatures and the LA92 driving cycle.

Table 1 shows the comparison between the CNN-UKF proposed in this article and other advanced methods under UDDS driving conditions. Among them, Ref. [27] uses standard LSTM to achieve SOC estimation. The study [28] uses a bidirectional GRU network to estimate SOC and SOE. In order to avoid the manual parameter adjustment, an improved pigeon genetic optimization algorithm is used to optimize the hyperparameters of the model automatically. Ref. [29] combined CNNs and Informer networks to achieve SOC estimation, and derived a Laplace-based loss function for training the network model composed of CNNs and Informer. The authors of [30] proposed the Fb-Ada-CNN-GRU-KF

method to estimate the SOC of the battery. As can be seen from Table 1, in the average prediction results of various temperatures, CNN-UKF has a lower RMSE and MAE, which are 0.00581 and 0.00467, respectively. Among these reference algorithms, all methods have achieved good SOC estimation results. Among them, the SOC estimation accuracy of [30] is the highest, and the average RMSE and MAE at different temperatures reached 0.00690 and 0.00543, respectively. Compared with the results of [30], the CNN-UKF method still has better estimation results, and the average values of RMSE and MAE are reduced by 15.80% and 14.00%, respectively.

**Table 1.** Experimental results obtained by different methods, under the UDDS driving cycle.

Method	Criterion	Temperature (°C)			Average
		25	10	0	
CNN	RMSE	0.01439	0.03134	0.03955	0.02843
	MAE	0.01142	0.02570	0.03337	0.02350
CNN-UKF	RMSE	0.00295	0.01140	0.00308	0.00581
	MAE	0.00209	0.00939	0.00253	0.00467
Method in [28]	RMSE	0.00937	0.01309	0.01827	0.01358
	MAE	0.00793	0.01023	0.01699	0.01172
Method in [27]	RMSE	0.0171	0.0324	/	0.02475
	MAE	0.0139	0.0266	/	0.02025
Method in [29]	RMSE	0.0062	0.0091	0.0108	0.00870
	MAE	0.0052	0.0087	0.0100	0.00797
Method in [30]	RMSE	0.0082	0.0078	0.0047	0.00690
	MAE	0.0070	0.0054	0.0039	0.00543

Table 2 shows the comparison between CNN-UKF and other methods under US06 driving conditions. It can be seen that compared with the method in [29], the average RMSE and MAE of CNN-UKF were reduced by 47.45% and 46.05%, respectively. Table 3 shows the comparison between CNN-UKF and other algorithms under NN driving conditions. It can be seen that compared with the method in [28], the average RMSE and MAE of CNN-UKF were reduced by 52.56% and 50.13%, respectively. Table 4 shows the comparison between CNN-UKF and other methods under LA92 driving conditions. It can be seen that compared with the method in [29], the average RMSE and MAE of CNN-UKF were reduced by 61.50% and 69.27%, respectively. It can be seen from Tables 1–4 that the same method under the same working conditions and different ambient temperatures leads to different estimation accuracy. Compared with other methods, the CNN-UKF has lower RMSE and MAE average values, which illustrates the effectiveness of the CNN-UKF proposed in this paper.

**Table 2.** Experimental results obtained by different methods, under the US06 driving cycle.

Method	Criterion	Temperature (°C)			Average
		25	10	0	
CNN	RMSE	0.02713	0.03889	0.04779	0.03794
	MAE	0.02169	0.03056	0.03866	0.03030
CNN-UKF	RMSE	0.00387	0.00497	0.00599	0.00494
	MAE	0.00337	0.00463	0.00593	0.00464
Method in [29]	RMSE	0.0069	0.0094	0.0119	0.00940
	MAE	0.0059	0.0089	0.0110	0.00860

**Table 3.** Experimental results obtained by different methods, under the NN driving cycle.

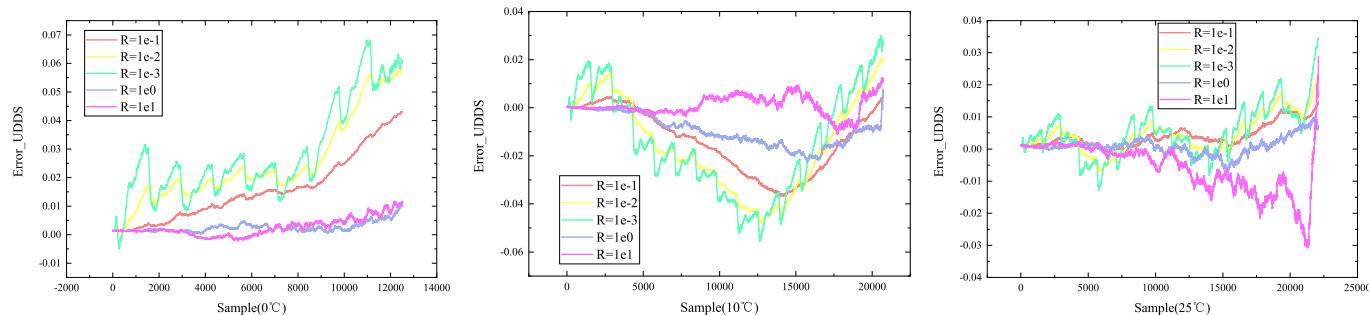
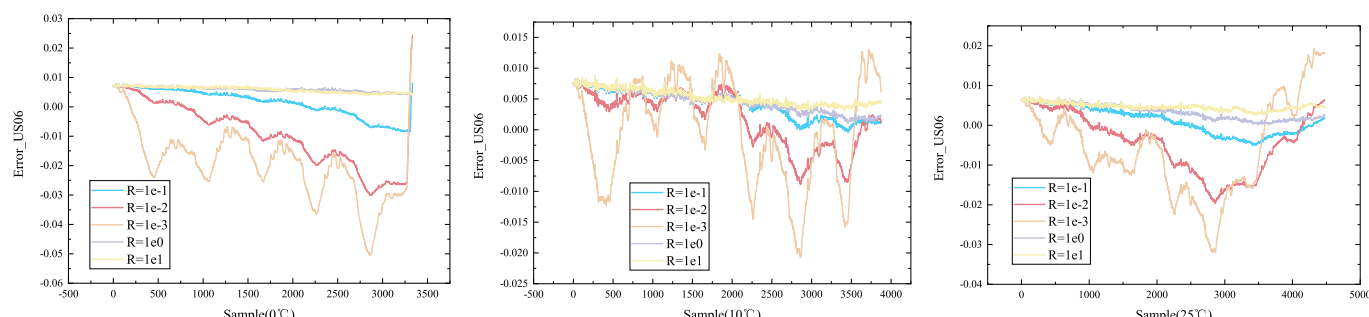
Method	Criterion	Temperature (°C)			Average
		25	10	0	
CNN	RMSE	0.03804	0.03528	0.05826	0.04386
	MAE	0.03152	0.02729	0.04793	0.03558
CNN-UKF	RMSE	0.00956	0.00398	0.00565	0.00640
	MAE	0.00875	0.00366	0.00500	0.00580
Method in [28]	RMSE	0.01229	0.01430	0.01388	0.01349
	MAE	0.01099	0.01300	0.01090	0.01163

**Table 4.** Experimental results obtained by different methods, under the LA92 driving cycle.

Method	Criterion	Temperature (°C)			Average
		25	10	0	
CNN	RMSE	0.03009	0.03159	0.03920	0.03363
	MAE	0.02645	0.02468	0.03106	0.02740
CNN-UKF	RMSE	0.00329	0.00412	0.00197	0.00313
	MAE	0.00276	0.00256	0.00116	0.00216
Method in [29]	RMSE	0.0069	0.0075	0.0100	0.00813
	MAE	0.0060	0.0069	0.0082	0.00703

### 3.3. Analysis of CNN-UKF Estimation SOC Results with Different Initial Values of $R$

To further verify the effect of CNN-UKF, this section sets different initial values of  $R$ , specifically,  $1 \times 10^{-1}$  (1e-1),  $1 \times 10^{-2}$  (1e-2),  $1 \times 10^{-3}$  (1e-3),  $1 \times 10^0$  (1e0) and  $1 \times 10^1$  (1e1), and tested under different driving conditions under temperature conditions of  $0^\circ\text{C}$ ,  $10^\circ\text{C}$  and  $25^\circ\text{C}$ . Figures 7–10 are the experimental error curves of CNN-UKF in UDDS driving conditions, US06 driving conditions, NN driving conditions and LA92 driving conditions, respectively. Tables 5–8 show the corresponding RMSE and MAE results.

**Figure 7.** Experimental results of CNN-UKF under UDDS conditions under different initial values of  $R$  and different temperature conditions.**Figure 8.** Experimental results of CNN-UKF under US06 conditions under different initial values of  $R$  and different temperature conditions.

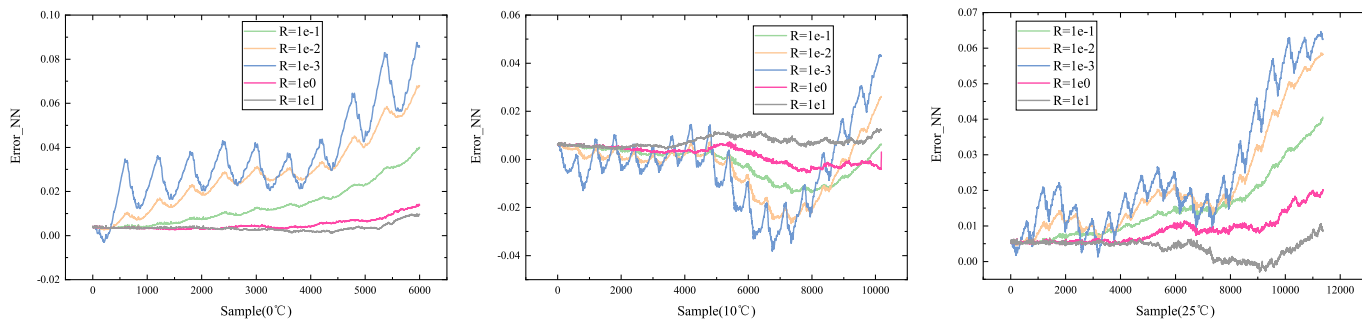


**Figure 9.** Experimental results of CNN-UKF under NN conditions under different initial values of  $R$  and different temperature conditions.

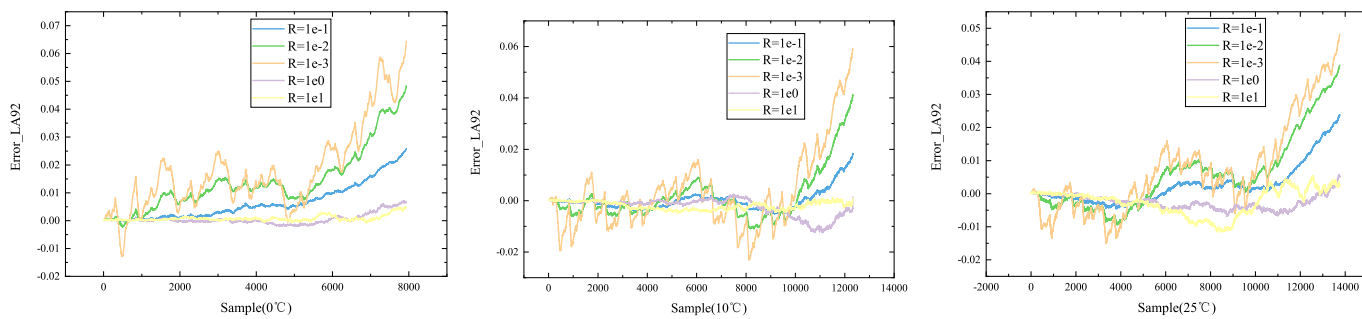


**Figure 10.** Experimental results of CNN-UKF under LA92 conditions under different initial values of  $R$  and different temperature conditions.

**Table 5.** Comparison of experimental results of different initial values of  $R$  under UDDS conditions.

Initial Value of $R$	Criterion	Temperature (°C)			Average
		25	10	0	
$1 \times 10^{-1}$	RMSE	0.00534	0.01898	0.01945	0.01459
	MAE	0.00407	0.01479	0.01573	0.01153
$1 \times 10^{-2}$	RMSE	0.00735	0.02444	0.02894	0.02024
	MAE	0.00567	0.02012	0.02477	0.01685
$1 \times 10^{-3}$	RMSE	0.00908	0.02599	0.03291	0.02266
	MAE	0.00703	0.02187	0.02839	0.01910
$1 \times 10^0$	RMSE	0.00295	0.01140	0.00308	0.00581
	MAE	0.00209	0.00939	0.00253	0.00467
$1 \times 10^1$	RMSE	0.00873	0.00418	0.00401	0.00564
	MAE	0.00631	0.00320	0.00297	0.00416

**Table 6.** Comparison of experimental results of different initial values of  $R$  under US06 conditions.

Initial Value of $R$	Criterion	Temperature (°C)			Average
		25	10	0	
$1 \times 10^{-1}$	RMSE	0.00361	0.00483	0.00491	0.00445
	MAE	0.00313	0.00424	0.00428	0.00388
$1 \times 10^{-2}$	RMSE	0.00865	0.00479	0.01433	0.00926
	MAE	0.00691	0.00427	0.01134	0.00751
$1 \times 10^{-3}$	RMSE	0.01303	0.00819	0.02275	0.01466
	MAE	0.01064	0.00685	0.02020	0.01256
$1 \times 10^0$	RMSE	0.00387	0.00497	0.00599	0.00494
	MAE	0.00337	0.00463	0.00593	0.00464
$1 \times 10^1$	RMSE	0.00473	0.00542	0.00592	0.00536
	MAE	0.00465	0.00527	0.00584	0.00525

**Table 7.** Comparison of experimental results of different initial values of  $R$  under NN conditions.

Initial Value of $R$	Criterion	Temperature (°C)			Average
		25	10	0	
$1 \times 10^{-1}$	RMSE	0.01771	0.00657	0.01666	0.01365
	MAE	0.01512	0.00539	0.01375	0.01142
$1 \times 10^{-2}$	RMSE	0.02576	0.01141	0.03162	0.02293
	MAE	0.02107	0.00801	0.02740	0.01883
$1 \times 10^{-3}$	RMSE	0.03027	0.01625	0.03972	0.02875
	MAE	0.02462	0.01198	0.03495	0.02385
$1 \times 10^0$	RMSE	0.00956	0.00398	0.00565	0.00640
	MAE	0.00875	0.00366	0.00500	0.00580
$1 \times 10^1$	RMSE	0.00456	0.00762	0.00389	0.00536
	MAE	0.00405	0.00736	0.00352	0.00498

**Table 8.** Comparison of experimental results of different initial values of  $R$  under LA92 conditions.

Initial Value of $R$	Criterion	Temperature (°C)			Average
		25	10	0	
$1 \times 10^{-1}$	RMSE	0.00652	0.00400	0.00907	0.00653
	MAE	0.00412	0.00262	0.00643	0.00439
$1 \times 10^{-2}$	RMSE	0.01249	0.00985	0.01790	0.01341
	MAE	0.00883	0.00637	0.01405	0.00975
$1 \times 10^{-3}$	RMSE	0.01575	0.01569	0.02357	0.01834
	MAE	0.01127	0.01080	0.01842	0.01350
$1 \times 10^0$	RMSE	0.00329	0.00412	0.00197	0.00313
	MAE	0.00276	0.00256	0.00116	0.00216
$1 \times 10^1$	RMSE	0.00467	0.00249	0.00128	0.00281
	MAE	0.00348	0.00203	0.00082	0.00211

It can be seen from Tables 5–8 that different initial values of  $R$  have an impact on the experimental results of CNN-UKF. Combining Tables 1–4, although the initial value of  $R$  will affect the effect of CNN-UKF, compared with CNN, the accuracy is still greatly improved. In experiments with different initial values of  $R$ , the maximum RMSE and MAE values of the UDDS working condition were 0.02266 and 0.01910, respectively, and the accuracy was improved by 20.30% and 18.72%, respectively, compared with the separate CNN model. The minimum RMSE and MAE are 0.00581 and 0.00467, respectively, and the accuracy is improved by 79.56% and 80.13%, respectively, compared with the simple CNN model. The maximum RMSE value and MAE value of the US06 working condition are 0.01466 and 0.01256, respectively, and the accuracy is improved by 61.36% and 58.55%, respectively compared with the simple CNN model. The minimum RMSE and MAE are 0.01466 and 0.01256, respectively, and the accuracy is improved by 88.27% and 87.19%, respectively, compared with the simple CNN model. The maximum RMSE value and MAE value of the NN working condition are 0.02875 and 0.02385, respectively, and the accuracy is improved by 34.45% and 32.97%, respectively, compared with the simple CNN model. The minimum RMSE and MAE are 0.00536 and 0.00498, respectively, and the accuracy is improved by 87.78% and 86.00%, respectively, compared with the simple CNN model. The maximum RMSE value and MAE value of LA92 working condition are 0.01834 and 0.01350, respectively, and the accuracy is improved by 45.47% and 50.73%, respectively, compared with the simple CNN model. The minimum RMSE and MAE are 0.00281 and 0.00211, respectively, and the accuracy is improved by 91.64% and 92.30%, respectively, compared with the simple CNN model. The improvement range of CNN-UKF compared to CNN model under different working conditions is more intuitively shown in Figure 11.

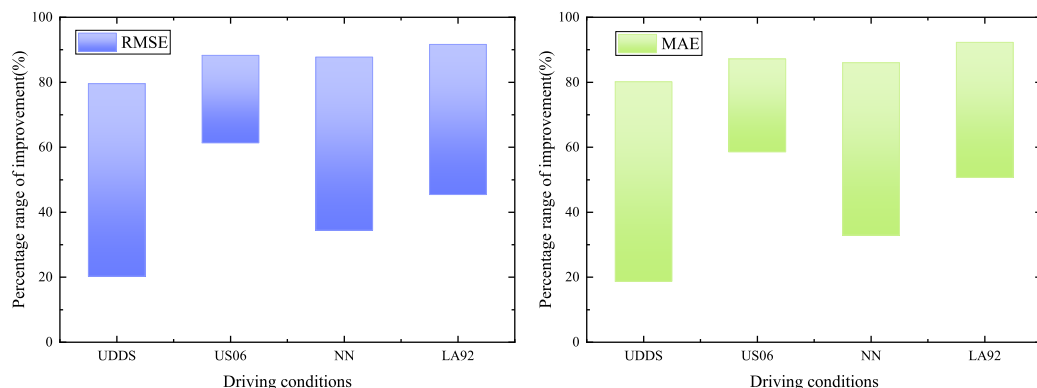


**Figure 11.** Experimental results of CNN-UKF under LA92 conditions under different initial values of  $R$  and different temperature conditions.

#### 4. Conclusions

The accurate prediction of SOC is very important for the BMS of LIBs. This paper proposed a CNN-UKF method to enhance the accuracy of existing SOC estimation approaches. The method takes advantage of the fact that neural networks do not need information about the complex chemical reactions inside the battery, and directly uses a CNN model to learn the nonlinear relationship between the LIB measurable data and SOC. In addition, to avoid the dependence of the neural network model on hyperparameter tuning, the method uses a UKF to filter the initial SOC estimations performed by the CNN. Experiments showed that the new CNN-UKF achieves high-precision SOC estimations, even without extensive hyperparameter tuning work. At the same time, experiments have also observed that the CNN-UKF method will also be affected by the initial value of  $R$  of UKF. Due to different initial values of  $R$ , the estimation effect of CNN-UKF will also be different. Compared with the simple CNN model, no matter what the initial value of  $R$  is, the accuracy is improved over the simple CNN model. In future work, we aim to develop models that are insensitive to filter parameters, thereby further enhancing the accuracy and robustness of SOC estimation.

**Author Contributions:** Methodology, L.C.; software, X.B.; validation and data curation, M.Z. and G.L.; writing—original draft preparation, H.M.; writing—review and editing, A.L. and L.C.; supervision and project administration, X.B. and A.L. All authors have read and agreed to the published version of the manuscript.

**Funding:** This research was funded by National Natural Science Funds of China (No. 62073114, No. 62341301), Anhui Provincial Key Research and Development Project (202304a05020060).

**Data Availability Statement:** Data used in this article are publicly available [26].

**Conflicts of Interest:** The authors declare no conflicts of interest.

#### References

- Shrivastava, P.; Naidu, P.A.; Sharma, S.; Panigrahi, B.K.; Garg, A. Review on technological advancement of lithium-ion battery states estimation methods for electric vehicle applications. *J. Energy Storage* **2023**, *64*, 107159. [[CrossRef](#)]
- Lu, J.; Wang, Z.; Zhang, Q.; Sun, C.; Zhou, Y.; Wang, S.; Qiu, X.; Xu, S.; Chen, R.; Wei, T. The effects of amino groups and open metal sites of MOFs on polymer-based electrolytes for all-solid-state lithium metal batteries. *Chin. J. Chem. Eng.* **2023**, *60*, 80–89. [[CrossRef](#)]
- Zhang, F.; Ye, W.; Lei, G.; Liu, Y.; Wang, X. SOH estimation of Li-ion battery based on FA-BPNN-K-means optimization algorithm. *J. Comput. Methods Sci. Eng.* **2022**, *22*, 1209–1222. [[CrossRef](#)]
- He, H.; Zhang, X.; Xiong, R.; Xu, Y.; Guo, H. Online model-based estimation of state-of-charge and open-circuit voltage of lithium-ion batteries in electric vehicles. *Energy* **2012**, *39*, 310–318. [[CrossRef](#)]
- Rahimi, M. Lithium-ion batteries: Latest advances and prospects. *Batteries* **2021**, *7*, 8. [[CrossRef](#)]
- Murawwat, S.; Gulzar, M.M.; Alzahrani, A.; Hafeez, G.; Khan, F.A.; Abed, A.M. State of charge estimation and error analysis of lithium-ion batteries for electric vehicles using Kalman filter and deep neural network. *J. Energy Storage* **2023**, *72*, 108039.

7. Li, S.; Ye, C.; Ding, Y.; Song, Y. Reliability assessment of renewable power systems considering thermally-induced incidents of large-scale battery energy storage. *IEEE Trans. Power Syst.* **2023**, *38*, 3924–3938. [[CrossRef](#)]
8. Zhang, M.; Wang, K.; Zhou, Y.T. Online state of charge estimation of lithium-ion cells using particle filter-based hybrid filtering approach. *Complexity* **2020**, *2020*, 8231243. [[CrossRef](#)]
9. Dini, P.; Colicelli, A.; Saponara, S. Review on Modeling and SOC/SOH Estimation of Batteries for Automotive Applications. *Batteries* **2024**, *10*, 34. [[CrossRef](#)]
10. Guo, P.; Wu, X.; Lopes, A.M.; Cheng, A.; Xu, Y.; Chen, L. Parameter identification for lithium-ion battery based on hybrid genetic-fractional beetle swarm optimization method. *Mathematics* **2022**, *10*, 3056. [[CrossRef](#)]
11. Snihir, I.; Rey, W.; Verbitskiy, E.; Belfadhel-Ayeb, A.; Notten, P.H. Battery open-circuit voltage estimation by a method of statistical analysis. *J. Power Sources* **2006**, *159*, 1484–1487. [[CrossRef](#)]
12. Ren, L.; Zhu, G.; Wang, J.V.; Luo, B.; Kang, J. Comparison of robustness of different state of charge estimation algorithms. *J. Power Sources* **2020**, *478*, 228767. [[CrossRef](#)]
13. Zhang, S.; Guo, X.; Zhang, X. An improved adaptive unscented Kalman filtering for state of charge online estimation of lithium-ion battery. *J. Energy Storage* **2020**, *32*, 101980. [[CrossRef](#)]
14. Zeng, Y.; Li, Y.; Yang, T. State of charge estimation for lithium-ion battery based on unscented Kalman filter and long short-term memory neural network. *Batteries* **2023**, *9*, 358. [[CrossRef](#)]
15. Hou, E.; Wang, Z.; Zhang, X.; Wang, Z.; Qiao, X.; Zhang, Y. Combined State of Charge and State of Energy Estimation for Echelon-Use Lithium-Ion Battery Based on Adaptive Extended Kalman Filter. *Batteries* **2023**, *9*, 362. [[CrossRef](#)]
16. Guo, S.; Ma, L. A comparative study of different deep learning algorithms for lithium-ion batteries on state-of-charge estimation. *Energy* **2023**, *263*, 125872. [[CrossRef](#)]
17. Liu, X.; Yang, J.; Wang, L.; Wu, J. Bayesian information criterion based data-driven state of charge estimation for lithium-ion battery. *J. Energy Storage* **2022**, *55*, 105669. [[CrossRef](#)]
18. Li, C.; Xiao, F.; Fan, Y. An approach to state of charge estimation of lithium-ion batteries based on recurrent neural networks with gated recurrent unit. *Energies* **2019**, *12*, 1592. [[CrossRef](#)]
19. Yang, F.; Li, W.; Li, C.; Miao, Q. State-of-charge estimation of lithium-ion batteries based on gated recurrent neural network. *Energy* **2019**, *175*, 66–75. [[CrossRef](#)]
20. Zhang, L.; Ji, T.; Yu, S.; Liu, G. Accurate prediction approach of SOH for lithium-ion batteries based on LSTM method. *Batteries* **2023**, *9*, 177. [[CrossRef](#)]
21. Li, J.; Jiang, Z.; Jiang, Y.; Song, W.; Gu, J. The State of Charge Estimation of Lithium-Ion Battery Based on Battery Capacity. *J. Electrochem. Soc.* **2023**, *169*, 120539. [[CrossRef](#)]
22. Che, Y.; Zheng, Y.; Wu, Y.; Lin, X.; Li, J.; Hu, X.; Teodorescu, R. Battery States Monitoring for Electric Vehicles Based on Transferred Multi-Task Learning. *IEEE Trans. Veh. Technol.* **2023**, *72*, 10037–10047. [[CrossRef](#)]
23. Ni, S.; Li, H. Battery state-of-charge prediction method based on one-dimensional convolutional neural network combined with long short-term memory network. *J. Comput. Appl.* **2021**, *41*, 1514.
24. Song, X.; Yang, F.; Wang, D.; Tsui, K.L. Combined CNN-LSTM network for state-of-charge estimation of lithium-ion batteries. *IEEE Access* **2019**, *7*, 88894–88902. [[CrossRef](#)]
25. Shahriar, S.M.; Bhuiyan, E.A.; Nahiduzzaman, M.; Ahsan, M.; Haider, J. State of charge estimation for electric vehicle battery management systems using the hybrid recurrent learning approach with explainable artificial intelligence. *Energies* **2022**, *15*, 8003. [[CrossRef](#)]
26. Kollmeyer, P. Panasonic 18650PF Li-ion battery data. 2018.
27. Ma, L.; Hu, C.; Cheng, F. State of charge and state of energy estimation for lithium-ion batteries based on a long short-term memory neural network. *J. Energy Storage* **2021**, *37*, 102440. [[CrossRef](#)]
28. Chen, L.; Song, Y.; Lopes, A.M.; Bao, X.; Zhang, Z.; Lin, Y. Joint estimation of state of charge and state of energy of lithium-ion batteries based on optimized bidirectional gated recurrent neural network. *IEEE Trans. Transp. Electrif.* **2023**, *10*, 1605–1616. . [[CrossRef](#)]
29. Zou, R.; Duan, Y.; Wang, Y.; Pang, J.; Liu, F.; Sheikh, S.R. A novel convolutional informer network for deterministic and probabilistic state-of-charge estimation of lithium-ion batteries. *J. Energy Storage* **2023**, *57*, 106298. [[CrossRef](#)]
30. Yang, Y.; Zhao, L.; Yu, Q.; Liu, S.; Zhou, G.; Shen, W. State of charge estimation for lithium-ion batteries based on cross-domain transfer learning with feedback mechanism. *J. Energy Storage* **2023**, *70*, 108037. [[CrossRef](#)]

**Disclaimer/Publisher’s Note:** The statements, opinions and data contained in all publications are solely those of the individual author(s) and contributor(s) and not of MDPI and/or the editor(s). MDPI and/or the editor(s) disclaim responsibility for any injury to people or property resulting from any ideas, methods, instructions or products referred to in the content.